Crystal chemistry and first principles studies of novel superhard tetragonal C7, C5N2, and C3N4

Samir Matar, Vladimir Solozhenko

Crystal chemistry and first principles studies of novel superhard tetragonal C_7, C_5N_2 and C_3N_4

Samir F. Matar [a] and Vladimir L. Solozhenko [b, *]

[a] Lebanese German University (LGU), Sahel Alma, Jounieh, Lebanon
https://orcid.org/0000-0001-5419-358X

[b] LSPM–CNRS, Université Sorbonne Paris Nord, 93430 Villetaneuse, France
https://orcid.org/0000-0002-0881-9761

Abstract

Tetragonal C_7, C_5N_2, and C_3N_4 characterized by mixed tetrahedral and trigonal atomic hybridizations, have been devised based on crystal chemistry rationale and structural optimization calculations within the Density Functional Theory (DFT). Substitution of $C(sp^2)$ and $C(sp^3)$ in C_7 for nitrogen yields α-C_5N_2 and β-C_5N_2, respectively, both of which are superhard, cohesive, and stable mechanically (elastic properties) and dynamically (phonon band structures). tet-C_3N_4 with both nitrogen sites within the C_7 structure was found to be cohesive and classified as ductile with Vickers hardness of 65 GPa. Due to the delocalization of π electrons of the sp^2-like hybridized atoms, metallic behavior characterizes all four phases.

Keywords: carbon nitrides; DFT; crystal structures; mechanical properties; phonons

* Corresponding author (e-mail: vladimir.solozhenko@univ-paris13.fr)

Introduction

Since the 1950s, interest has focused on carbon allotropes, especially those that resemble diamond in hardness and other electronic properties, such as diamond at the nanoscale for applications in electronics [1]. Expanding to carbon's neighbors, B and N, a superhard cubic boron nitride was synthesized in 1957 [2], which often replaces diamond in tools because it is more stable at high temperatures, although its hardness is less than that of diamond. As for binary compounds of the C-N system, ultrahard phases of C_3N_4 stoichiometry have been predicted already in the 1990s [3,4], with allegedly higher bulk moduli and hardness than those of diamond due to the short and strong C-N bonds. However, the existence of such phases has been strongly questioned, and even in the case of experimentally synthesized C-N phases, their stoichiometry and structures are still controversial due to the heterogeneity of the samples obtained. In particular, it should be noted that strong N–N repulsions induced by short N–N nonbonded distances do not favor the synthesis of the nitrogen-rich C-N phases, especially when CVD and PVD methods are used. The hypothesis of gaseous carbon dinitrogen release during vapor phase deposition led to the proposal of model systems such as CN_2 [5,6], based on studies within the well-established quantum mechanics framework of the density functional theory (DFT) [7,8].

Thus, the search for new C-N phases is mainly limited to the carbon-rich system (i.e., N/C < 1), where many hypothetical binary compounds have been predicted in recent years, such as rhombohedral and cubic $C_{17}N_4$ [9]; cubic C_4N [9]; monoclinic [10] and orthorhombic [11] C_3N; tetragonal and orthorhombic $C_{11}N_4$ [12]; cubic α-C_3N_2 and β-C_3N_2 [13]; cubic C_4N_3 [14]; orthorhombic CN [15], etc. Among the hypothetical nitrogen-rich C-N phases, only CN_2 is worth mentioning, whose stability has been predicted over a wide range of pressures [16]. However, none of these many predicted structures has been synthesized, with the sole exception of the orthorhombic CN [17] and diamond-like C_2N [18]. The progress and problems in predicting novel ultrahard binary and ternary phases of the B-C-N system from first principles in conjunction with available experimental data have been recently discussed in our review paper [19].

In the present paper, we further develop the problem of carbon nitrides, which remains of great interest, as follows from recent works [20,21]. In the framework of accurate DFT calculations, we have designed a new cohesive and stable (mechanically and dynamically) tetragonal heptacarbon (C_7) allotrope, characterized by both tetrahedral (sp^3-like) and trigonal (sp^2-like) carbon sites, which was used as a template for selective substitutions of carbon for nitrogen, leading to two new carbon-rich nitrides of C_5N_2 stoichiometry, as well as to a new tetragonal C_3N_4.

Computational framework

The identification of the ground state structures corresponding to the energy minima and prediction of their mechanical and dynamical properties were carried out by DFT-based calculations using the Vienna Ab initio Simulation Package (VASP) code [22,23] and the projector augmented wave (PAW) method [23,24] for the atomic potentials. Exchange correlation (XC) effects were considered using the generalized gradient functional approximation (GGA) [25]. Relaxation of the

atoms to the ground state structures was performed with the conjugate gradient algorithm according to Press *et al*. [26]. The Blöchl tetrahedron method [27] with corrections according to the Methfessel and Paxton scheme [28] was used for geometry optimization and energy calculations, respectively. Brillouin-zone (BZ) integrals were approximated by a special **k**-point sampling according to Monkhorst and Pack [29]. Structural parameters were optimized until atomic forces were below 0.02 eV/Å and all stress components were < 0.003 eV/Å^3. The calculations were converged at an energy cutoff of 400 eV for the plane-wave basis set in terms of the **k**-point integration in the reciprocal space from $k_x(6)\times k_y(6)\times k_z(4)$ up to $k_x(12)\times k_y(12)\times k_z(8)$ for the final convergence and relaxation to zero strains. In the post-processing of the ground state electronic structures, the charge density projections were operated on the carbon atomic sites. The charge density was analyzed using Bader's atoms in molecules (AIM) theory [30] to assess the trends of charge transfer. The elastic constants C_{ij} were calculated to evaluate the mechanical stability and hardness as described in detail below in the "Mechanical properties" section. The dynamic stabilities were evaluated from the phonon band structures according to Togo *et al*. [31]. The electronic band structures were obtained using the all-electron DFT-based ASW method [32] and the GGA XC functional [25]. The VESTA (Visualization for Electronic and Structural Analysis) program [33] was used to visualize the crystal structures and charge densities.

Results and discussion

Crystal chemistry and structure characterization.

The calculated structures at energy minima from fully geometry-optimized setups are detailed in Table 1 and the structures are shown in Fig. 1. The body-centered tetragonal 'neoglitter' C_6 [34] has been used to devise novel carbon allotrope, tetragonal C_7. The 'neoglitter' structure, shown in ball-and-stick and polyhedral representations, consists of *C4* tetrahedra at the 8 corners and body-center, connected by C-C pairs along the vertical direction. C_6 is then expressed as $(C_{tet})_2(C_{trg})_4$ as made up of tetrahedral and trigonal sites, readily available to be used as a template for CN_2 carbon dinitride. However, such hypothesis was rejected as preliminary calculations resulted in a weakly cohesive compound (-0.62 eV/atom) compared to the magnitudes of the other dinitrides in Table 1. Furthermore, the CN_2 dinitride was characterized by unstable dynamic behavior due to negative phonons.

The novel C_7 consists of an elongated tetragonal box with tetrahedral carbon atoms occupying the 8 corners as in 'neoglitter' and in-between trigonal carbons leading to a loss of the body-centered character with subsequent change of space group *I*-4*m*2 (No. 119). The fully optimized geometry structure is shown in Fig. 1b, and the polyhedral representation on the right highlights the sp^3-sp^2 hybrid structure of C_7 with tetrahedral and trigonal motifs. The first data column of Table 1 provides the numerical description of the structure inscribed as the following phases in the tetragonal *P*-4*m*2 (No. 115) space group. Four different carbon sites build the structure. The *C4* tetrahedra have an angle of 106.5°, slightly different from the perfect 109.47° of C(sp^3), and the corresponding distance is d(C-C) = 1.52 Å, also smaller than in diamond (1.54 Å). The other shorter

distances correspond to the vertical C-C bonds. Subtracting the atomic C contribution of -6.6 eV from the total energy gives an atomic average cohesive energy of -2.09 eV/atom. This value is lower than the cohesive energy of diamond (2.49 eV/atom).

Substitution of C for N was performed along with two working hypotheses to obtain the stoichiometry of C_5N_2:

- The first hypothesis was to create a dinitride with N-N pairs as shown in Fig. 1c, where the white spheres represent the N@C (2e) 0,0,z (Table 1, 2nd data column). After geometry optimization, the final structure shows little deviation from pristine C_7, as can be seen from the internal parameters, while the distances show a short d(N-N) = 1.36 Å, larger than the length of the N≡N bond (~1.09 Å) in the N_2 molecule. The volume is smaller, resulting in a slightly higher density. The atom-averaged cohesive energy is significantly reduced compared to C_7, but the carbonitride labeled α-C_5N_2 remains cohesive with E_{coh}/atom = -1.50 eV/at.
- The second hypothesis was to replace N@C (2g) ½, 0, z (Table 1, 3rd data column), thus creating *CN4* tetrahedra at the 8 corners as schematically shown in Fig. 1d. Therefore, d(C-N) = 1.49 Å is shorter than in C_7 and α-C_5N_2. The remarkable result of such β-C_5N_2 is the higher (by 0.23 eV) cohesive atomic energy of this configuration, which is clearly more favorable than that of α-C_5N_2. Finally, the density is higher, 3.252 g/cm^3. Therefore, the tetrahedral configuration prevails.

Finally, we found that the simultaneous N@C (2g) and N@C (2e) substitutions resulted in the known C_3N_4 nitrogen-rich stoichiometry. The structure thus constructed was then calculated for the sake of completeness. The results given in the last column of Table 1 are also presented in Fig. 1e, with N shown as red spheres. The structure shows a small d(N-N) and the volume is the smallest, resulting in the highest density. The cohesive energy is smaller than those of both α-C_5N_2 and β-C_5N_2. C_3N_4 proposed by Teter and Hemley [4], calculated for comparison, gives a cohesive energy of -1.29 eV/atom, i.e. more cohesive than *tet*-C_3N_4 (Table 1).

Simulated X-ray diffraction patterns of three new phases are shown in Fig. 2. It is easy to see that they all have the same topology, which is significantly different from the diamond topology.

Trends of charge transfer

For Pauling negativities: χ_N=3.04 and χ_C=2.55, charge transfers from C to N of different magnitudes are expected. From the high BZ integration, the charge density output (CHGCAR) was analyzed based on the AIM theory according to Bader [30]. The analyses of the carbon nitrides studied showed a small amount of charge transfer.

In α-C_5N_2: $\Delta Q_C = 0.676$, $\Delta Q_N = -1.69$; in β-C_5N_2: $\Delta Q_C = 0.588$, $\Delta Q_N = -1.47$; and in *tet*-C_3N_4: $\Delta Q_C = 2.22$; $\Delta Q_N = -1.67$. Regarding C_7, despite the different atomic positions and chemical behaviors as sp^3/sp^2, the charge transfers were found to be negligible letting the allotrope be considered as a covalent chemical system. Both C_5N_2 polymorphs can be considered as polar

covalent, but the large amount of charge transfer in *tet*-C_3N_4 allows it to be characterized as ionocovalent, reinforced by the large number of electrons transferred from C to N. Mechanical and dynamic properties of the novel phases were further analyzed.

Mechanical properties

Elastic constants

The mechanical properties were obtained by determining the elastic constants from the strain-stress relationship. For the tetragonal crystal systems, the terms of mechanical stability are defined by elastic constants C_{ij} as follows:

$$C_{ii}\ (i = 1, 3, 4, 6) > 0;\ \ C_{11} > C_{12},\ \ C_{11} + C_{33} - 2C_{13} > 0;\ \ 2C_{11} + C_{33} + 2C_{12} + 4C_{13} > 0$$

The calculated C_{ij} of C_7 and new carbon nitrides are given in Table 2. All values are positive, and their combinations given above obey the rules of mechanical stability. The bulk (B_V) and shear (G_V) moduli were calculated by Voigt averaging the single-crystal elastic constants using ELATE software [35]. As a general trend, the bulk moduli are close to 390 GPa for β-C_5N_2 and *tet*-C_3N_4, proportional to their densities, and close to 360 GPa for C_7 and α-C_5N_2, which have lower densities. The shear moduli of the new phases are close to 230 GPa, except for a slightly lower value of 205 GPa for *tet*-C_3N_4. There is a general trend of the Pugh modulus ratio (G_V/B_V) < 1 with the lowest value of 0.52 for *tet*-C_3N_4. This is indicative of ductile systems with low brittleness, probably due to the presence of trigonal atomic fragments in the structures of all phases.

Hardness

To estimate the Vickers hardness (H_V) of the proposed new phases, two contemporary theoretical models were used. The thermodynamic (T) model [36], which is based on thermodynamic properties and crystal structure, generally shows perfect agreement with experimental data and is therefore recommended for hardness evaluation of superhard phases [19]. The Lyakhov-Oganov (LO) model [37] considers the topology of the crystal structure, the strength of covalent bonding, the degree of ionicity and directionality. As shown earlier [19], empirical models using the elastic properties are not reliable in the case of superhard compounds of light elements, so we have not considered these models. Fracture toughness (K_{Ic}) was evaluated using the Mazhnik-Oganov model [38]. The results for the currently proposed phases compared to the properties of diamond and hypothetical cubic C_3N_4 [3] are summarized in Tables 3 and 4.

The hardness of tetragonal C_7 is the highest of all the new phases, but it is ~15% less than that of diamond. This is to be expected since the density of this phase is significantly lower (by a factor of 1.2). The hardness of the three new C-N phases is even lower and is ~65 GPa for all of them, closer to the hardness of cubic C_3N_4 [3].

The elastic moduli of all four new phases are close, with the Pugh modulus ratio (G/B) being less than 1 and varying from 0.52 for *tet*-C_3N_4 to 0.64 for C_7.

These trends in mechanical properties are consistent with the fact that nitrogen plays a major role in the softening structures of the three C-N compounds, while the presence of trigonal carbon in all new phases further reinforces this tendency.

Dynamical properties with the phonons

To verify the dynamic stability of the new phases, the phonon band structures were calculated. The methodology consists in calculating the phonon modes by finite displacements of the atoms from the equilibrium position found by the preliminary optimization of the crystal geometry - another heavier method exists as Density Functional Perturbation Theory (DFPT). This leads the forces on all atoms constituting the crystal structure to raise off their equilibrium positions. Analysis of the forces associated with a systematic set of displacements yields a series of phonon frequencies. The phonon dispersion curves along the main lines of the tetragonal Brillouin zone (BZ) are then obtained using the Python code "Phonopy" (see [31] for further details).

Figure 3 shows the phonon band structures for the new carbon allotrope and carbon nitrides phases that develop along the main lines of the primitive tetragonal Brillouin zone.

Frequencies (ω) expressed in units of THz are along the vertical direction. In all four panels the frequencies are positive, providing the signature of dynamically stable systems. Between 0 and ~10 THz, the first three bands correspond to lattice rigid translations: two in-plane and one out-of-plane; they are labeled as acoustic modes. At higher energies and up to the highest ω, the remaining bands are the optical modes. Knowing that diamond has the highest band observed by Raman spectroscopy at ω~40 THz [41], all frequency maxima of the four phases in Figs. 2a, 2b, 2c, 2d, are above this magnitude, up to ω~49 THz for α-C_5N_2 (Fig. 3b), assigned to the N-N stretching. Then, while diamond has pure sp^3 hybridization, the currently studied C_7 and new carbon nitrides have mixed sp^3/sp^2 hybridization, the latter leading to high frequencies for the very short distances (Table 1).

Electronic band structures

Figure 4 shows the electronic band structure plots obtained using the all-electron DFT-based augmented spherical method (ASW) [32] and the GGA exchange correlation DFT functional. In all four panels along the vertical direction of the energy, there is a continuous development of bands. Consequently, there is no separation (gap) between the valence band (VB) filled with electrons and the empty conduction band (CB), indicating metallic-like behavior. Then the zero energy is with respect to the Fermi level (E_F). Such electronic behavior can be attributed to the delocalization induced by the π electrons of the sp^2-like hybridized atoms present in all systems. Insulating behavior requires electron localization as found in diamond, which is known to be an electronic

insulator with a wide band gap of ~5 eV between VB and CB. In fact, diamond is characterized only by tetrahedral C(sp^3).

Density of states (DOS)

For a better assessment of the role of each site and chemical constituent in the electronic structure and further on the band structures, the density of states DOS was calculated and plotted. The energy reference is now along the *x*-axis. As in the band structures, the zero energy is considered with respect to the Fermi level E_F, visualized by a straight vertical red line. Along the *y*-axis the DOS are in units of 1/eV. Fig. 5a, showing C_7 DOS, exhibits a continuous skyline of the different constituents' valence states from the lowest VB energy (-22 eV - -15 eV) where s states predominate, to up to -5 eV where p states predominate. Such similar shapes of the site-resolved DOS are indicative of quantum mixing of the respective valence states describing the chemical bonding. From -5 eV up to E_F, lower intensity DOS of C1 is observed with almost zero intensity at E_F, while the other C DOS show large intensity at E_F. This illustrates the different behavior of tetrahedral C1 versus trigonal C2.

Upon introduction of nitrogen (C_5N_2, Fig. 5b & c), additional features appear with a broadening of VB by almost 5 eV due to the larger electronegativity of N compared to C. VB is divided into s-like VB (from -27 eV to -20 eV) dominated by N DOS, and the part with p-states (-20 eV - E_F), which also shows dominant N states. Less intense states are found at E_F, mainly originating from C2, indicating s-like conductivity. Additionally, in Fig. 5d, the C_3N_4 DOS show increasingly larger nitrogen contribution throughout VB and above E_F, in CB.

Conclusions

The presence of mixed sp^3/sp^2 carbon hybridization in novel tetragonal C_7 allotrope allowed to devise three new carbon nitrides along hypotheses related to selective occupations of either atomic site. Two C_5N_2 phases were found to be mechanically and dynamically stable with more cohesive tetrahedral *CN4* phase than the phase with linear N-N motifs. Tetragonal C_3N_4 was similarly devised by allowing N to occupy both sp^3 and sp^2 carbon sites in C_7, resulting in ductile metallic phase. C_7 was found to be cohesive and classified as ductile with Vickers hardness of 65 GPa. The ductility was found to be enhanced with a decrease of the Pugh modulus ratio G/B along the series from 0.65 to 0.52 with resultant decrease in hardness. Due to the delocalization of π electrons of the sp^2-like hybridized atoms, metallic behavior characterizes all four phases. If synthesized, either as bulk by solid-state synthesis at high pressures and high temperatures, or by sputtering and other deposition techniques, the new phases are likely to improve our understanding of the long-standing problem of nitrogen chemistry in carbon nitrides.

Annex 1

Crystal structures publications in the Cambridge Crystallographic Data Centre (CCDC):

C_7 : Deposition No 2255470. Refcode: JIJCUE. DOI: 10.5517/ccdc.csd.cc2fq039

α-C_5N_2 : Deposition No 2252296. Refcode: DIMGOZ. DOI: 10.5517/ccdc.csd.cc2flpqg

β-C_5N_2 : Deposition No 2252297. Refcode: DIMGUF. DOI: 10.5517/ccdc.csd.cc2flprh

***tet*-C_3N_4** : Deposition No 2271012. Refcode: TINMIQ. DOI: 10.5517/ccdc.csd.cc2g75gc

References

[1] Qin, J.-X.; Yang, X.-G.; Lv, C.-F.; Li, Y.-Z.; Liu, K.-K.; Zang, J.-H.; Yang, X.; Dong, L.; Shan. C.-X. Nanodiamonds: Synthesis, properties, and applications in nanomedicine. *Mater. Des.* **2021**, *210*, 110091.

[2] Wentorf, R.H. Cubic form of boron nitride. *J. Chem. Phys.* **1957**, *26*, 956.

[3] Liu, A.; Wentzcovitch, R. Stability of carbon nitride solids. *Phys. Rev. B* **1994**, *50*, 10362-10365.

[4] Teter, D.; Hemley, R. Low-compressibility carbon nitrides. *Science* **1996**, *271*, 53–55.

[5] Weihrich R., Eyert V., Matar S.F. Structure and electronic properties of new model dinitride systems: a density-functional study of CN_2, SiN_2, and GeN_2. *Chem. Phys. Lett.* **2003**, *373*, 636–641.

[6] Weihrich R., Matar S.F., Betranhandy E., Eyert V. A model study for the breaking of N_2 from CN_x within DFT. *Solid State Sci.* **2003**, *5*, 701–703.

[7] Hohenberg, P.; Kohn, W. Inhomogeneous electron gas. *Phys. Rev. B* **1964**, *136*, 864–871.

[8] Kohn, W.; Sham, L. Self-consistent equations including exchange and correlation effects. *Phys. Rev. A* **1965**, *140*, 1133–1138.

[9] Li, Z.; Luo, K.; Liu, B.; Sun, L.; Ying, P.; Liu, C.; Hu, W.; He, J. Superhard carbon-rich C-N compounds hidden in compression of the mixture of carbon black and tetracyanoethylene. *Carbon* **2021**, *184*, 846-54.

[10] Li, X.; Xing, M Novel carbon-rich nitride C_3N: A superhard phase in monoclinic symmetry. *Comp. Mater. Sci.* **2019**, *158*, 170-177.

[11] Hao, J.; Liu, H.; Lei, W.; Tang, X.; Lu, J.; Liu, D.; Li, Y. Prediction of a superhard carbon-rich C-N compound comparable to diamond. *J. Phys. Chem. C* **2015**, *119*, 28614-28619.

[12] Ding, Y. Mechanical properties and hardness of new carbon-rich superhard $C_{11}N_4$ from first-principles investigations, *Physica B* **2012**, *407*, 2282-2288.

[13] Tian, F.; Wang, J.; He, Z.; Ma, Y.; Wang, L.; Cui, T.; Chen, C.; Liu, B.; Zou, G. Superhard semiconducting C_3N_2 compounds predicted via first-principles calculations. *Phys. Rev. B* **2008**, *78*, 235431

[14] Qian, Y.; Wu, H. D-C_4N_3: a superhard ferromagnetic half-metal predicted by first-principles study. *Phys. Lett. A* **2022**, *423*, 127814.

[15] Wang, X. Polymorphic phases of sp^3-hybridized superhard CN. *J. Chem. Phys.* **2012**, *138*, 184506.

[16] Dong, H.F.; Oganov, A.R.; Zhu, Q.; Qian, G.R. The phase diagram and hardness of carbon nitrides. *Sci. Rep.* **2015**, *5*, 9870.

[17] Stavrou, E.; Lobanov, S.; Dong, H.; Oganov, A.R.; Prakapenka, V.B.; Konopkova Z.; Goncharov, A.F. Synthesis of ultra-incompressible sp^3-hybridized carbon nitride with 1:1 stoichiometry. *Chem. Mater.* **2016**, *28*, 6925-6933.

[18] Komatsu, T. Shock synthesis and characterization of new diamond-like carbon nitrides. *Phys. Chem. Chem. Phys.* **2004**, *6*, 878-880.

[19] Solozhenko, V.L; Matar, S.F. Prediction of novel ultrahard phases in the B-C-N system from first principles: Progress and problems. *Materials* **2023**, *16*, 886.

[20] Pickard, C.J.; Salamat, A.; Bojdys, M.J.; Needs, R.J.; McMillan, P.F. Carbon nitride frameworks and dense crystalline polymorphs. *Phys. Rev. B* **2016**, *94*, 094104.

[21] Talukdar, M.; Deb, P. Recent progress in research on multifunctional graphitic carbon nitride: An emerging wonder material beyond catalyst. *Carbon* **2022**, *192*, 308-331.

[22] Kresse, G.; Furthmüller, J. Efficient iterative schemes for ab initio total-energy calculations using a plane-wave basis set. *Phys. Rev. B* **1996**, *54*, 11169.

[23] Kresse, G.; Joubert, J. From ultrasoft pseudopotentials to the projector augmented wave. *Phys. Rev. B* **1999**, *59*, 1758–1775.

[24] Blöchl, P.E. Projector augmented wave method. *Phys. Rev. B* **1994**, *50*, 17953–17979.

[25] Perdew, J.; Burke, K.; Ernzerhof, M. The Generalized Gradient Approximation made simple. *Phys. Rev. Lett.* **1996**, *77*, 3865–3868.

[26] Press, W.; Flannery, B.; Teukolsky, S.; Vetterling, W. Numerical Recipes, 2nd ed.; Cambridge University Press: New York, NY, USA, 1986.

[27] Blöchl, P.; Jepsen, O.; Anderson, O. Improved tetrahedron method for Brillouin-zone integrations. *Phys. Rev. B* **1994**, *49*, 16223–16233.

[28] Methfessel, M.; Paxton, A. High-precision sampling for Brillouin-zone integration in metals. *Phys. Rev. B* **1989**, *40*, 3616–3621.

[29] Monkhorst, H.; Pack, J. Special k-points for Brillouin Zone integration. *Phys. Rev. B* **1976**, *13*, 5188–5192.

[30] Bader, R.F.W. A bond path: a universal indicator of bonded interactions. *J. Phys. Chem. A* **1998**, *102*, 7314–7323.

[31] Togo, A.; Tanaka, I. First principles phonon calculations in materials science. *Scr. Mater.* **2015**, *108*, 1–5.

[32] Eyert, V. Basic notions and applications of the augmented spherical wave method. *Int. J. Quantum Chem.* **2000**, *77*, 1007–1031.

[33] Momma, K.; Izumi F. VESTA3 for three-dimensional visualization of crystal, volumetric and morphology data. *J. Appl. Crystallogr.* **2011**, *44*, 1272-1276.

[34] Matar, S.F.; Solozhenko, V.L. Novel ultrahard sp^2/sp^3 hybrid carbon allotrope from crystal chemistry and first principles: body centered tetragonal C_6 ('neoglitter'). *Diamond Relat. Mater.* **2023**, *133*, 109747.

[35] Gaillac, R.; Pullumbi, P.; Coudert, F.-X. ELATE: an open-source online application for analysis and visualization of elastic tensors. *J. Phys.: Condens. Matter* **2016**, *28*, 275201.

[36] Mukhanov, V.A.; Kurakevych, O.O.; Solozhenko, V.L. The interrelation between hardness and compressibility of substances and their structure and thermodynamic properties. *J. Superhard Mater.* **2008**, *30*, 368-378.

[37] Lyakhov, A.O.; Oganov, A.R. Evolutionary search for superhard materials: Methodology and applications to forms of carbon and TiO_2. *Phys. Rev. B* **2011**, *84*, 092103.

[38] Mazhnik, E.; Oganov, A.R. A model of hardness and fracture toughness of solids. *J. Appl. Phys.* **2019**, *126*, 125109.

[39] Bindzus, N.; Straasø, T.; Wahlberg, N.; Becker, J.; Bjerg, L.; Lock, N.; Dippel, A.-C.; Iversen, B.B. Experimental determination of core electron deformation in diamond. *Acta Cryst. A* **2014**, *70*, 39-48.

[40] Brazhkin, V.V.; Solozhenko, V.L. Myths about new ultrahard phases: Why materials that are significantly superior to diamond in elastic moduli and hardness are impossible. *J. Appl. Phys.* **2019**, *125*, 130901.

[41] Krishnan, R.S. Raman spectrum of diamond. *Nature* **1945**, *155*, 171.

Table 1. Crystal structure parameters of new tetragonal (*P*-4*m*2) phases.

	C_7	α-C_5N_2	β-C_5N_2	*tet*-C_3N_4
a (Å)	2.5290	2.5262	2.4929	2.4848
c (Å)	7.3720	7.1428	7.2279	7.1433
C1 (1*a*) 0,0,0	✓	✓	✓	✓
C2 (2*g*) ½,0,z	z=0.3039	z=0.1158	z=0.3050	z=0.3094
C(N) (2*g*) ½,0,z	z=0.1146	(C) z=0.3057	(N) z=0.113	(N) z=0.1138
C'(N') (2e) 0,0,z	z=0.3991	(N') z=0.4043	(C) z=0.3977	(N') z=0.4053
Cell volume ($Å^3$)	47.15	45.58	44.92	44.10
Density (g/cm^3)	2.961	3.208	3.256	3.466
Bond length (Å)	1.396 1.454 1.521	1.356 (C-C) 1.367 (N-N) 1.446 (C-N) 1.510 (C-C)	1.389 (C-N) 1.415 (C-C) 1.476 (C-C) 1.491 (C-N)	1.353 (N-N) 1.412 (C-N) 1.485 (C-N)
E_{total} (eV)	-60.88	-57.13	-58.70	-54.23
E_{coh}/atom (eV)	-2.09	-1.50	-1.73	-1.03

Table 2. Elastic constants and bulk (B_V) and shear (G_V) moduli (in GPa) of new tetragonal phases. *G/B* is the Pugh modulus ratio.

	C_{11}	C_{12}	C_{13}	C_{33}	C_{44}	C_{66}	B_V	G_V	G_V/B_V
C_7	771	14	122	1224	78	138	365	238	0.65
α-C_5N_2	738	20	92	1375	43	88	362	220	0.61
β-C_5N_2	832	20	145	1264	80	98	394	230	0.58
tet-C_3N_4	542	154	282	1027	127	217	394	205	0.52

Table 3. Vickers hardness (H_V) and bulk moduli (B_0) of carbon allotropes and carbon nitrides calculated in the framework of the thermodynamic model of hardness [36]

	Space group	$a = b$ (Å)	c (Å)	ρ (g/cm^3)	H_V (GPa)	B_0 (GPa)
Diamond	*Fd*-3*m*	3.56661[*]		3.517	98	445[†]
C_7 [#115]	*P*-4*m*2	2.5290	7.3720	2.961	82	373
α-C_5N_2 [#115]	*P*-4*m*2	2.5262	7.1428	3.208	65	383
β-C_5N_2 [#115]	*P*-4*m*2	2.4929	7.2279	3.256	66	389
tet-C_3N_4 [#115]	*P*-4*m*2	2.4848	7.1433	3.466	65	385
c-C_3N_4 [#215] [3]	*P*-43*m*	3.4300 [3]		3.788	71	421

[*] Ref. 39

[†] Ref. 40

Table 4 Mechanical properties of carbon allotropes and carbon nitrides: Vickers hardness (H_V), bulk modulus (B), shear modulus (G), Young's modulus (E), Poisson's ratio (ν) and fracture toughness (K_{Ic})

	H_V		B		G_V	E[‡]	ν[‡]	K_{Ic}[§]
	T[*]	LO[†]	B_0[*]	B_V				
	GPa							MPa·m$^{1/2}$
Diamond	98	90	445[**]		530[**]	1138	0.074	6.4
C_7 [#115]	82	76	373	365	238	586	0.232	4.7
α-C_5N_2 [#115]	65	64	383	362	220	549	0.247	4.2
β-C_5N_2 [#115]	66	69	389	394	230	577	0.256	4.9
tet-C_3N_4 [#115]	65	67	385	394	205	524	0.278	4.8
c-C_3N_4 [#215] [3]	71	73	421	422[††]	397[††]	907	0.142	7.2

[*] Thermodynamic model [36]

[†] Lyakhov-Oganov model [37]

[‡] E and ν values calculated from elastic constants using ELATE software [35]

[§] Mazhnik-Oganov model [38]

[**] Ref. 40

[††] Calculated from the literature data on elastic constants [3] using the Voigt approach

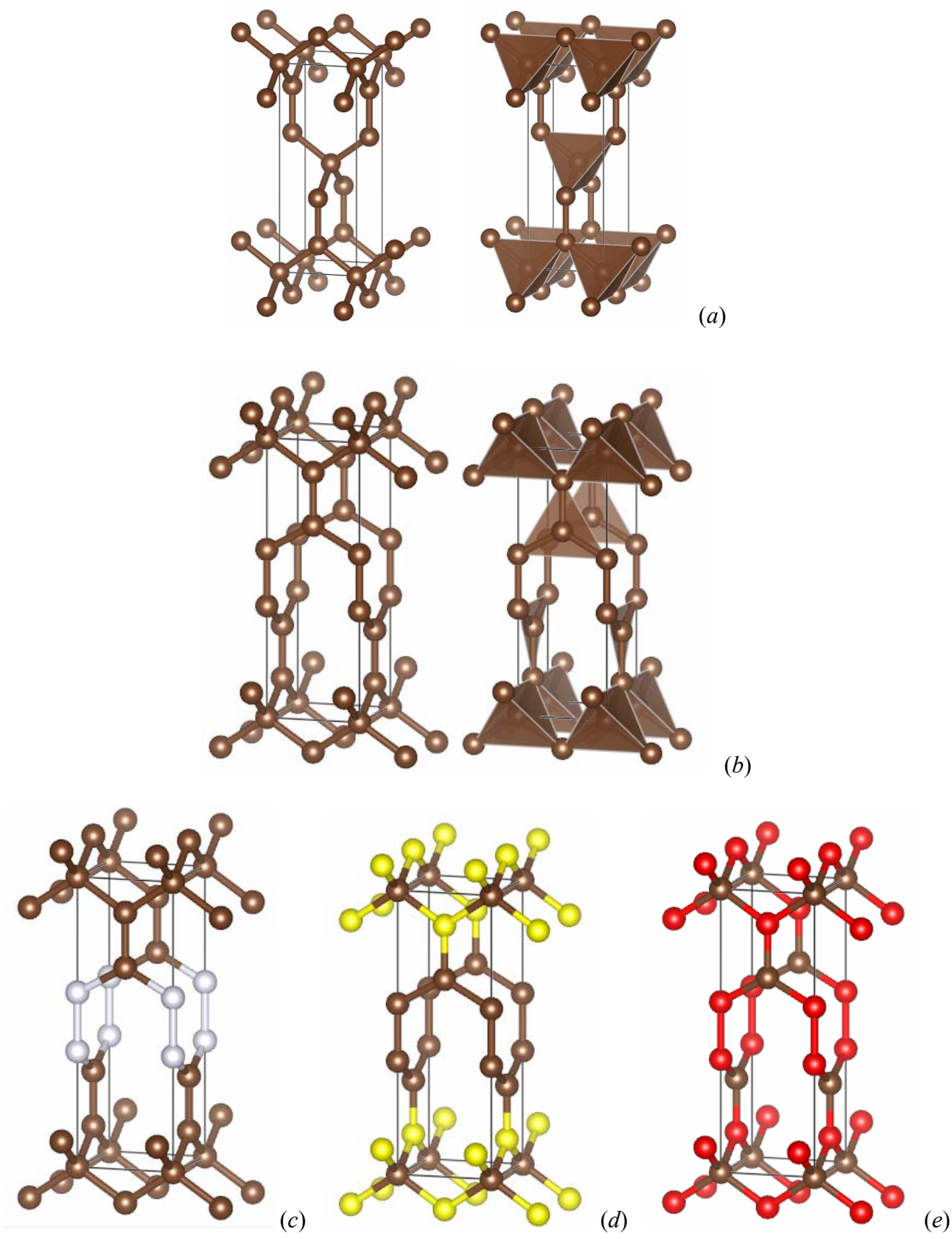

Fig. 1 'Neoglitter' C_6 [34] (*a*) and tetragonal C_7 (*b*) with ball-and-stick and polyhedral representations; α-C_5N_2 with linear N-N fragments (white spheres) (*c*); *tet*-C_5N_2 with nitrogen forming *CN4* tetrahedra (yellow spheres) (*d*); and *tet*-C_3N_4 with red (regrouping white+yellow) nitrogen spheres (*e*).

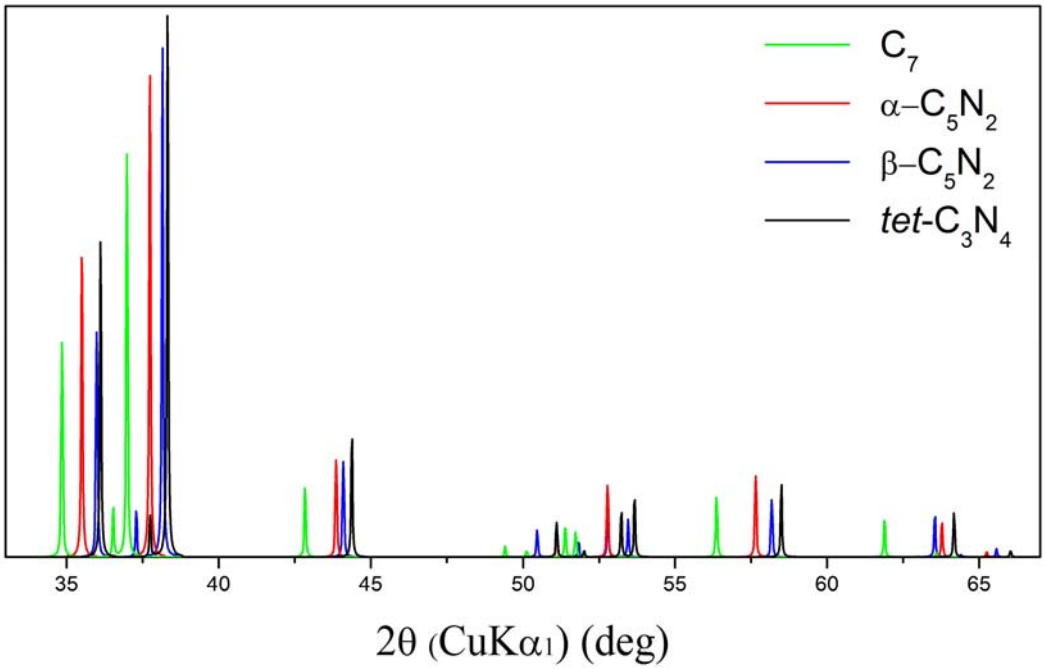

Fig. 2 Simulated X-ray diffraction patterns of new tetragonal phases.

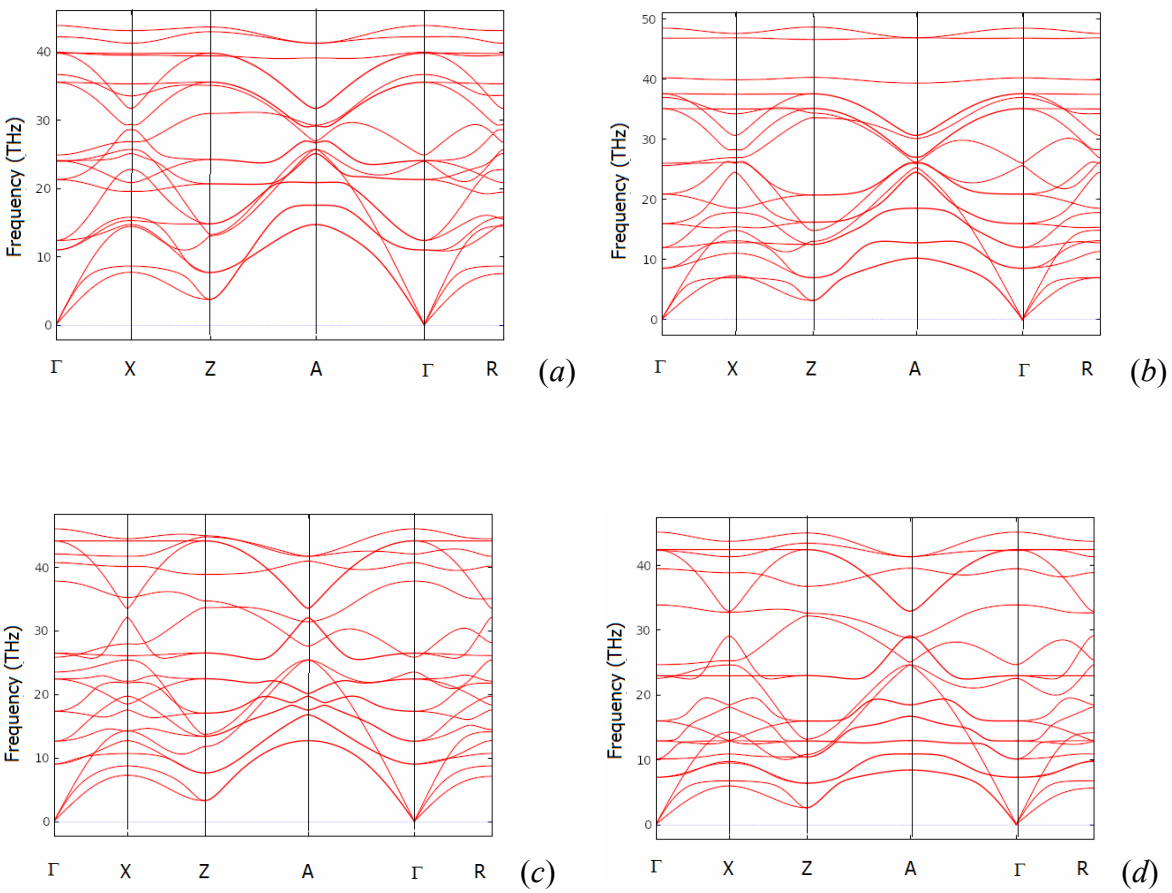

Fig. 3 Phonon band structures of tetragonal C_7 (*a*), α-C_5N_2 (*b*), *tet*-C_5N_2 (*c*) and *tet*-C_3N_4 (*d*).

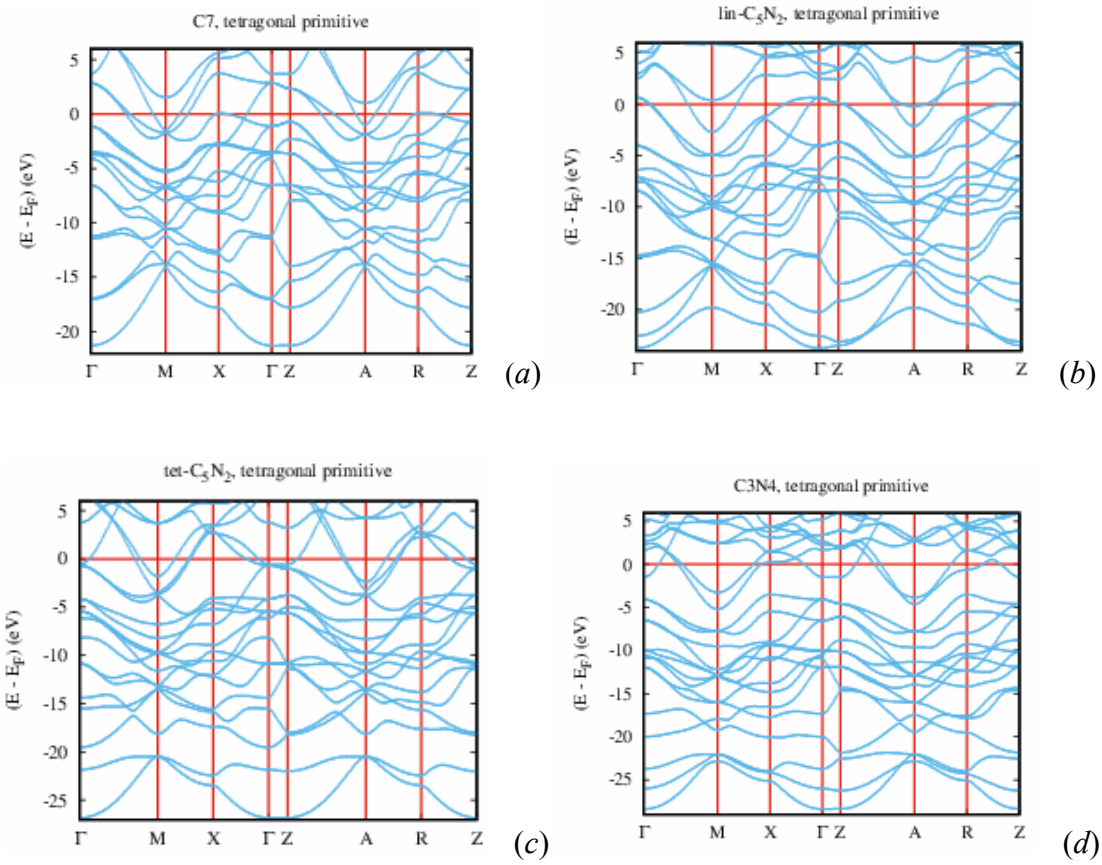

Fig. 4 Electronic band structures of tetragonal C_7 (*a*), α-C_5N_2 (*b*), *tet*-C_5N_2 (*c*) and *tet*-C_3N_4 (*d*).

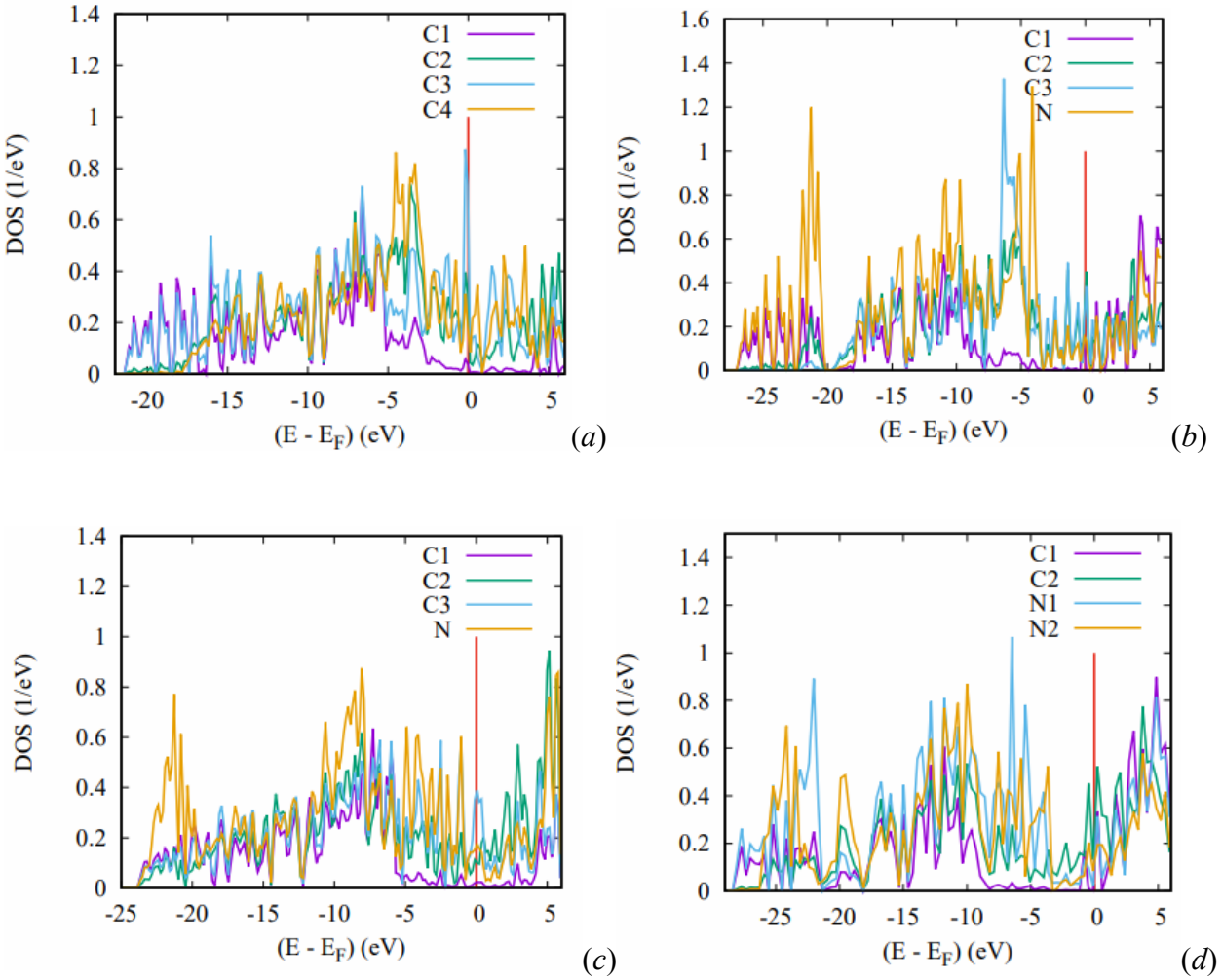

Fig. 5 Site projected density of states (DOS) of tetragonal C_7 (*a*), α-C_5N_2 (*b*), β-C_5N_2 (*c*) and *tet*-C_3N_4 (*d*).